ELSEVIER

Journal of Alloys and Compounds 408–412 (2006) 649–652

Journal of ALLOYS AND COMPOUNDS

www.elsevier.com/locate/jallcom

Oxide ionic conductivity of apatite-type lanthanum silicates

H. Yoshioka *

Hyogo Prefectural Institute of Technology, 3-1-12 Yukihira-cho, Suma-ku, Kobe 654-0037, Japan

Received 30 July 2004; received in revised form 26 October 2004; accepted 15 December 2004
Available online 7 July 2005

Abstract

Dense ceramic disks of apatite-type lanthanum silicates have been prepared using sol–gel derived powders by sintering at first 1600 °C and then 1750 °C. AC impedance measurements showed that the oxide ionic conductivity of $La_xSi_6O_{1.5x+12}$ increases from ∼1 mS cm^{-1} to a maximum of ∼20 mS cm^{-1} with increasing the La content from $x = 9.29$ to 9.92. Rietveld refinements revealed that the observed powder X-ray diffraction patterns fit to a defect structure model which incorporates La ions into 4f cation vacancy of the apatite phase and contains extra oxide ions in an interstitial site near the conduction channel. The observed increase in the conductivity with the La content is explained by an interstitial conduction mechanism associated with an increase in the extra oxide ions.

Keywords: Ionic conduction; Sol–gel synthesis; X-ray diffraction

1. Introduction

A number of oxide ion conductors have been developed for an application as solid electrolytes of solid oxide fuel cells (SOFCs). Among them, lanthanum silicates with an apatite-type structure are considered as potential candidates for SOFCs operating at intermediate temperature (600–800 °C), because they have high ionic conductivity of 10–20 mS cm^{-1} at 800 °C and low activation energy of about 0.6 eV [1].

A conduction mechanism of the apatite-type lanthanum silicates is also of interest; oxide ions are considered to migrate via a conduction channel along the *c*-axis of an apatite-type structure with an interstitial mechanism [2] rather than a vacancy mechanism which accounts for high ionic conductivity of typical oxide ion conductors such as fluorite-type Y_2O_3 stabilized ZrO_2 (YSZ) and perovskite-type $L_{1-x}Sr_xGa_{1-y}Mg_yO_z$ (LSGM).

The structure of the apatite-type lanthanum silicate is shown in Fig. 1 [1,3]. There are six isolated SiO_4 tetrahedrons in the $P6_3/m$ unit cell. La ions occupy in the seven-coordinated 6h and nine-coordinated 4f sites. Two oxide ions locate in the conduction channel. The composition without extra oxide ions is $La_{9.33}Si_6O_{26}$, which contains 6.7% of cation vacancies. If the vacancies are filled with La ions, extra oxide ions should be introduced to interstitial sites. The extra ions existing near the conduction channel may enhance the ionic conductivity. This interstitial conduction mechanism [2] suggests that the ionic conductivity of the lanthanum silicates should be greatly affected by the La content. Nakayama and Sakamoto have shown that $La_{10}Si_6O_{27}$ gives higher ionic conductivity than $La_{9.33}Si_6O_{26}$ [1]. However, $La_{10}Si_6O_{27}$ tends to contain a minor impurity phase [1], which has prevented precise structural analysis. Therefore, discussions are limited to a single-phase region near $La_{9.33}Si_6O_{26}$ [3,4]; no unambiguous discussion on the interstitial conduction mechanism in relation to the La content has been presented. In this study, we report on the ionic conductivity and the defect structure model in relation to the La content to elucidate the conduction mechanism of the apatite-type lanthanum silicates.

2. Experimental

A sol–gel method was employed to improve homogeneity of the samples [2,5]; lanthanum nitrate and tetraethyl orthosilicate (TEOS) were used as starting materials to

* Tel.: +81 78 731 4487; fax: +81 78 736 3777.
E-mail address: hide@hyogo-kg.go.jp.

0925-8388/$ – see front matter © 2005 Elsevier B.V. All rights reserved.
doi:10.1016/j.jallcom.2004.12.180

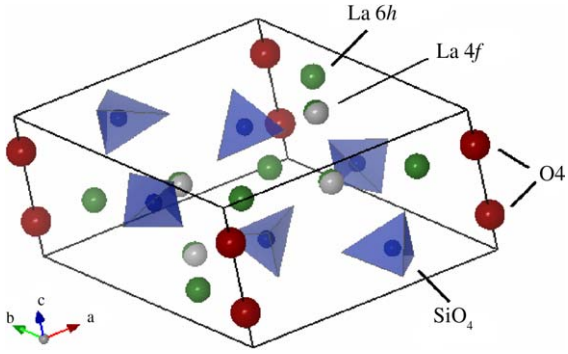

Fig. 1. The structure of an apatite-type $La_{9.33}Si_6O_{26}$.

obtain $La_xSi_6O_{1.5x+12}$ powders ($8.96 \leq x \leq 10.57$). The calcined powders were pressed into disks and subjected to sintering. The disks were very porous after the first sintering at 1600 °C for 4 h. Therefore, the second sintering was performed at 1750 °C for 4 h to obtain dense ceramic disks having bulk densities of more than 85%. MgO stabilized ZrO_2 setters, which greatly reduce reactions between disks and setters during the sintering [1] were used. Both faces of the disks were polished, painted with Pt paste and fired at 1000 °C. AC impedance was measured at temperatures from room temperature to 900 °C over frequencies ranging from 100 MHz to 0.1 Hz using a Solartron 1260 impedance analyzer. The chemical compositions were calculated from weight ratios of the starting materials and a conversion factor which were previously determined for the selected composition ($x = 9.92$) using inductively coupled plasma (ICP) spectroscopy. The structure was investigated from the Rietveld analysis of the powder X-ray diffraction (XRD) patterns obtained at room temperature using RIETAN-2000 [6].

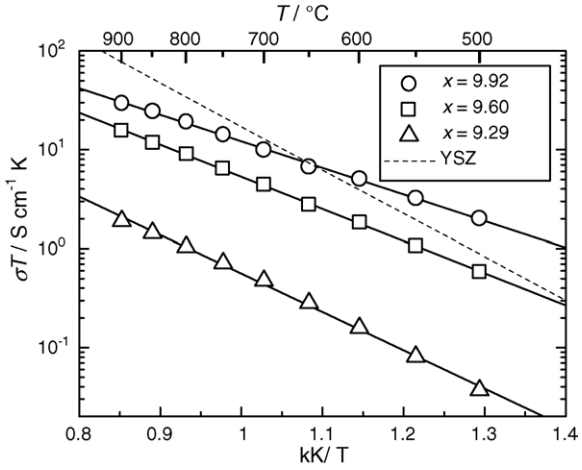

Fig. 3. Temperature variation of the bulk conductivity of $La_xSi_6O_{1.5x+12}$ ($x = 9.29$, 9.60 and 9.92).

3. Results and discussion

3.1. Ionic conductivity

Fig. 2 shows the impedance plots of a sample ($x = 9.60$) at different temperatures. The impedance response at 300 °C (Fig. 2(a)) consists of three semicircles corresponding to an equivalent circuit having a bulk, a grain boundary (gb) and an electrode interface contribution (Fig. 2(d)). The bulk and grain boundary semicircles which appear at high frequency get remarkably smaller at 500 °C (Fig. 2(b)). Only a lower-frequency semicircle attributable to the electrode interface appears at 800 °C (Fig. 2(c)). The temperature variation of the impedance response is similar to that reported by Tao and Irvine [2]. Bulk conductivity was calculated from the resistance corresponding to the bulk semicircle; for the plot

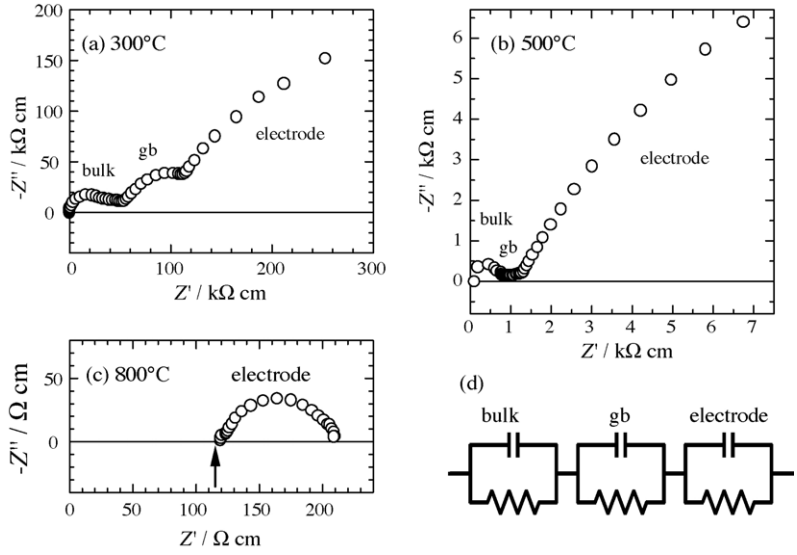

Fig. 2. The impedance plots of $La_xSi_6O_{1.5x+12}$ ($x = 9.60$) at different temperatures and the equivalent circuit.

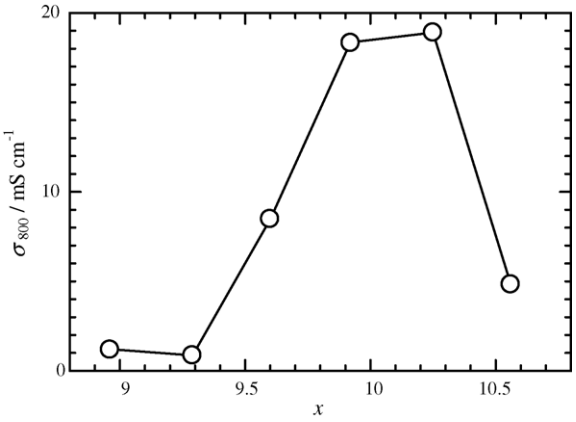

Fig. 4. Bulk conductivity of $La_xSi_6O_{1.5x+12}$ measured at 800 °C as a function of the La content.

like Fig. 2(c), however, the resistance at a higher-frequency intercept as shown by an arrow was used.

Fig. 3 displays a temperature variation of the bulk conductivity for $x = 9.29$, 9.60 and 9.92. The conductivity of ZrO_2–8% Y_2O_3 (YSZ) is also included for comparison. Obviously, the La content greatly affects value and slope of the conductivity; with increasing the La content, the conductivity increases and the activation energy decreases as 0.77, 0.64 and 0.53 eV for $x = 9.29$, 9.60 and 9.92, respectively. Consequently, the bulk conductivity of $x = 9.92$ is considerably high at low temperatures, showing higher conductivity than YSZ below 650 °C.

The compositional dependence of the conductivity is clearly shown in Fig. 4, where the bulk conductivity at 800 °C is plotted in a linear scale against the La content. It remains almost constant at $\sim$1 mS cm^{-1} when $x \leq 9.29$, increases rapidly at $9.29 < x < 9.92$ and shows high conductivity of $\sim$20 mS cm^{-1} around $9.92 \leq x \leq 10.25$. It decreases again at $x > 10.25$. It is clear that the conductivity shows a maximum at the La content of $\sim$10. This compositional dependence is in accord with the previous report of Nakayama and Sakamoto [1], supporting the model that the extra oxide ions introduced by the La incorporation into 4f cation vacancy enhance oxide ion migration [2].

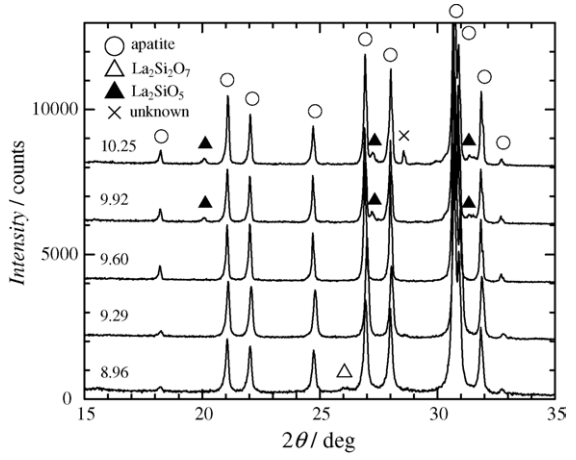

Fig. 5. XRD patterns of $La_xSi_6O_{1.5x+12}$ ($8.96 \leq x \leq 10.25$).

3.2. Structure analysis

Fig. 5 shows XRD patterns of the samples with different La contents. An apatite phase formed as a dominant phase in all compositions prepared. Minor impurity phases of La_2SiO_5 and $La_2Si_2O_7$ are observed with $x = 9.92$ and 8.96, respectively. The apatite single-phase range of $9.29 \leq x \leq 9.60$ prepared by the sol–gel preparation is identical with $9.33 \leq x \leq 9.62$ prepared by solid state reactions [4], showing no significant improvement by the sol–gel preparation.

Table 1
Refined structural parameters for $La_xSi_6O_{1.5x+12}$

	$x = 9.29$	$x = 9.60$	$x = 9.92$
a (Å)	9.7178(2)	9.7137(3)	9.7162(3)
c (Å)	7.1813(1)	7.1879(2)	7.1932(2)
V (Å^3)	587.31(2)	587.36(3)	588.10(3)
R_{wp} (%)	14.48	13.14	13.79
R_p (%)	11.24	9.84	10.65
R_e (%)	7.57	7.86	7.53
R_I (%)	6.25	6.41	8.86
S	1.91	1.67	1.83
La1, 6h (x y 1/4)			
x	0.2304(2)	0.2270(2)	0.2282(2)
y	−0.0125(3)	−0.0134(2)	−0.0110(3)
B (Å^2)	0.61(3)	0.77(3)	0.54(3)
La2, 4f (1/3 2/3 z)			
g	0.8215[a]	0.9[a]	0.98[a]
z	0.0013(7)	−0.0022(5)	0.0009(6)
B (Å^2)	1.04(5)	1.17(4)	1.68(5)
Si, 6h (x y 1/4)			
x	0.3999(9)	0.4024(8)	0.4031(8)
y	0.3652(9)	0.3708(8)	0.3709(8)
B (Å^2)	0.04(16)	0.73(14)	−0.17(14)
O1, 6h (x y 1/4)			
x	0.3128(20)	0.3435(17)	0.3317(22)
y	0.4815(19)	0.4895(16)	0.4863(18)
B (Å^2)	1.04(20)	0.81(15)	0.54(17)
O2, 6h (x y 1/4)			
x	0.6001(20)	0.5868(16)	0.6318(21)
y	0.4775(21)	0.4722(17)	0.5005(19)
B (Å^2)	=B(O1)	=B(O1)	=B(O1)
O3, 12i (x y z)			
x	0.3250(11)	0.3369(10)	0.3412(12)
y	0.2531(13)	0.2577(10)	0.2603(13)
z	0.0883(13)	0.0703(11)	0.0915(13)
B (Å^2)	=B(O1)	=B(O1)	=B(O1)
O4, 2a (0 0 1/4)			
g	0.9646[a]	1.0[a]	1.0[a]
B (Å^2)	1.13(58)	2.67(56)	3.69(72)
O5, 12i (0.1 0.23 0.62)			
g	–	0.0333[a]	0.0733[a]
B (Å^2)	–	=B(O4)	=B(O4)

[a] Fixed from the composition.

In order to reveal the influence of the La content on the defect structure and the conductivity, Rietveld analyses of the XRD patterns have been performed for $x = 9.29$ ($\sim$1 mS cm^{-1} at 800 °C), 9.60 ($\sim$10 mS cm^{-1} at 800 °C) and 9.92 ($\sim$20 mS cm^{-1} at 800 °C). Although the XRD patterns were obtained at room temperature, a compositional dependence of the conductivity is fundamental as can be seen from the temperature variation in Fig. 3. The refined structural parameters obtained are listed in Table 1. All atomic positions are very similar to those obtained by the neutron powder diffraction [3,4]. All La ion vacancies of $x = 9.29$ locate in the 4f site, which is also in accordance with the previous reports [3,4]. In addition, a good fit has been obtained for the structure model of $x = 9.29$ having no extra oxide ion and slight oxide vacancy in the O4 site as can be expected from the composition, $La_{9.29}(SiO_4)_6O_{1.93}$.

For $x = 9.60$ ($La_{9.60}(SiO_4)_6O_{2.40}$), with a decrease in the La ion vacancy, interstitial oxide ions are assumed to exist. However, it was impossible to determine the interstitial position from the powder XRD data, thus we put the extra oxide ions to an interstitial O5 site (0.01 0.23 0.62) which was predicted to be most energetically favorable from atomistic simulations [7] and investigated an improvement of the fit. A reliability factor, R_{wp}, decreases from 14.15 to 13.14% when all extra oxide ions occupy the O5 sites, indicating that the extra ions seem to be in the peripheral of the conduction channel.

For $x = 9.92$, the apatite phase with an almost fully occupied 4f site and increasing amount of interstitial O5 ions gives a best fit, though the sample contains a little amount of the impurity phase. The role of 4f cation vacancy to the ionic conductivity of the apatite-type lanthanum silicates has been discussed frequently [3,4]. The fact that $x = 9.92$ gives the highest conductivity, however, reveals an importance of the interstitial oxide ions rather than the existence of the 4f cation vacancy. Details of the Rietveld refinements will be published elsewhere.

4. Conclusion

(1) The oxide ionic conductivity of apatite-type lanthanum silicates is strongly affected by the La content; it increases from $\sim$1 to $\sim$20 mS cm^{-1} at 800 °C with the La content increasing from 9.29 to 9.92.
(2) The powder XRD patterns fit well to a defect structure model, which has decreasing 4f cation vacancy and increasing extra oxide ions at an interstitial site near the conduction channel with increasing the La content.
(3) The observed increase in the conductivity with the La content is due to extra oxide ions existing near the conduction channel via an interstitial conduction mechanism.

References

[1] S. Nakayama, M. Sakamoto, J. Eur. Ceram. Soc. 18 (1998) 1413–1418.
[2] S. Tao, J.T.S. Irvine, Mater. Res. Bull. 36 (2001) 1245–1258.
[3] J.E.H. Sansom, D. Richings, P.R. Slater, Solid State Ionics 139 (2001) 205–210.
[4] L. León-Reina, E.R. Losilla, M. Martínez-Lara, S. Bruque, M.A.G. Aranda, J. Mater. Chem. 14 (2004) 1142–1149.
[5] H. Yoshioka, Chem. Lett. 33 (2004) 392–393.
[6] F. Izumi, T. Ikeda, Mater. Sci. Forum 321–324 (2000) 198–205.
[7] J.R. Tolchard, M.S. Islam, P.R. Slater, J. Mater. Chem. 13 (2003) 1956–1961.